Supporting Information

Solid acids with SO_3H groups and tunable surface properties: versatile catalysts for biomass conversion

Patrícia A. Russo, Margarida M. Antunes, Patrícia Neves, Paul V. Wiper, Enza Fazio, Fortunato Neri, Francesco Barreca, Luís Mafra, Martyn Pillinger, Nicola Pinna and Anabela A. Valente

1. TGA curves of the prepared materials

Thermogravimetric analysis of the composites showed that the carbon starts to thermally degrade above 275-300 °C, and is completely decomposed at 600-650 °C (Figure S1, SI). The onset temperature of the major weight loss in the TGA curves of the samples, associated with the degradation of the carbon, depends on the sample. For samples CST-0 and CST-0.1, this temperature is above 300 °C, while it decreases down to 276 °C for CST-1 probably because the latter has a higher amount of surface acid sites that may lead to autocatalytic decomposition of the carbon. This effect has been observed before for carbons with high contents of surface functionalities.[1, 2]

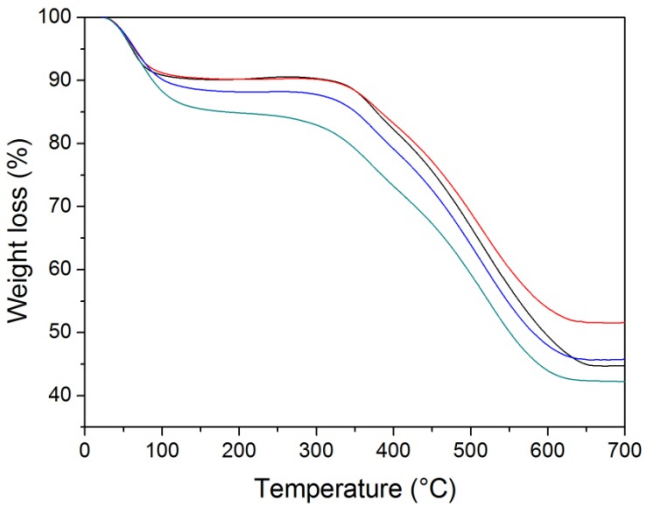

Figure S1. Thermogravimetric curves in air of the composite materials CST-0 (black), CST-0.1 (red), CST-0.4 (blue) and CST-1 (green).

2. N_2 adsorption-desorption isotherm of the silica support and composites

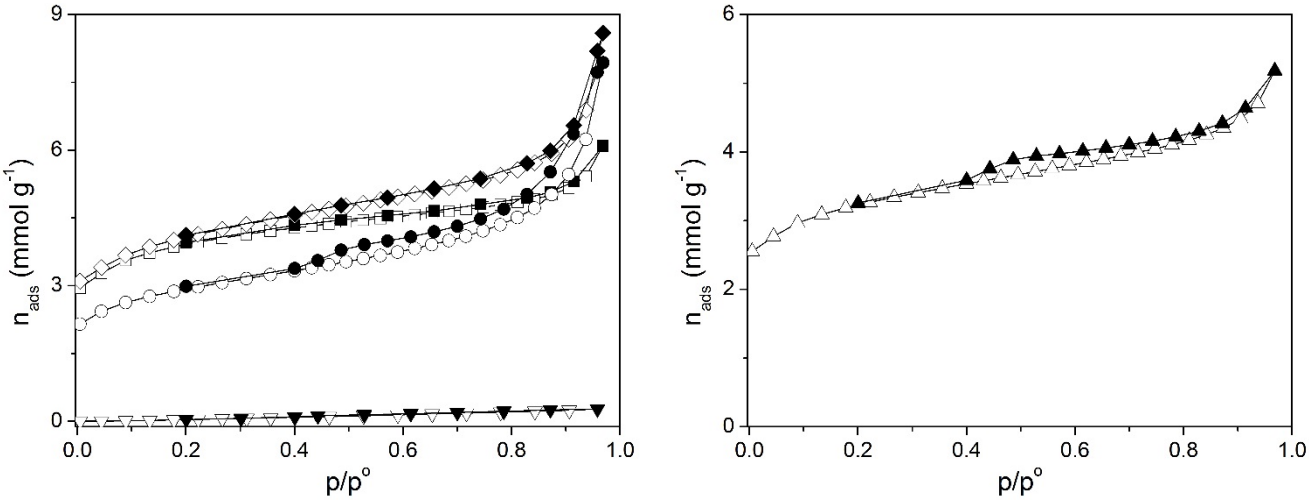

Figure S2. Nitrogen adsorption-desorption isotherms, at -196 °C, of CST-0.1 (◊), CST-0 (□), CST-0.4 (Δ), CST-1 (○) and CT-1 (▽) (open symbols-adsorption; closed symbols-desorption).

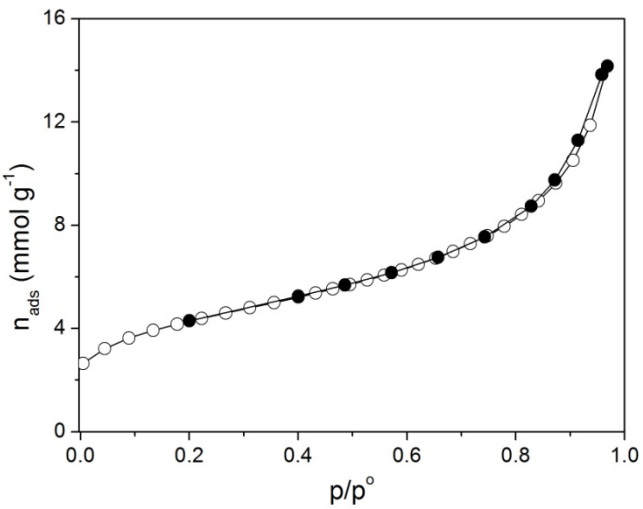

Figure S3. Nitrogen adsorption-desorption isotherm at -196 °C of the commercial silica used to synthesize the composites. The silica used as support is non-porous (A_{BET}=346 m^2 g^{-1}).

3. Powder X-ray diffraction patterns of the prepared materials

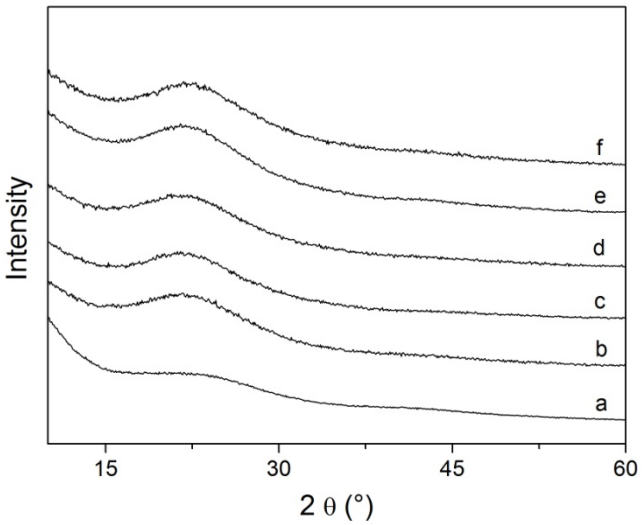

Figure S4. Powder X-ray diffraction patterns of a) CT-1, b) CST-0-600, c) CST-0, d) CST-0.1, e) CST-0.4 and f) CST-1.

4. Raman spectra of selected CST materials

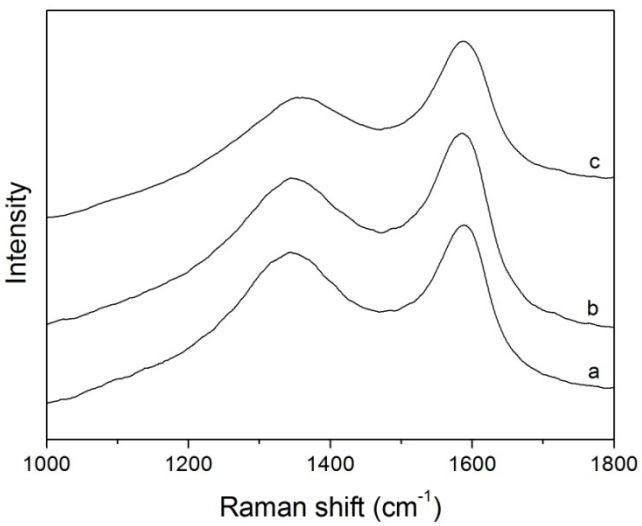

Figure S5. Raman spectra of a) CST-0-600, b) CST-0 and c) CST-1.

5. FT-IR spectra of the silica support and CST-0-600

The spectrum of the pristine silica exhibits bands at 1101 and 808 cm^{-1} associated with the stretching of the Si-O-Si bonds, and a band at 468 cm^{-1} attributed to the bending of Si-O-Si bonds. The band at 970 cm^{-1} corresponds to the bending of silanol bonds Si-O-H.

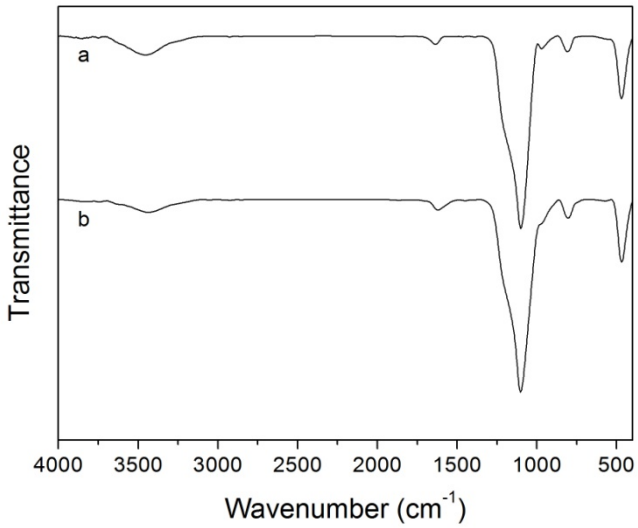

Figure S6. FT-IR spectra of the a) silica support and b) CST-0-600.

6. ^{13}C CP MAS NMR

The ^{1}H-^{13}C CP MAS spectrum of CST-nc/a exhibits very sharp, well-defined resonances. The peaks between 144 and 125 ppm arise from the nonequivalent aromatic carbons of the TsOH molecule, in particular the resonance at 139 ppm is assigned to the aromatic carbons bonded to the -SO_3H groups. The resonance at 21.5 ppm corresponds to the aliphatic carbon in the compound.

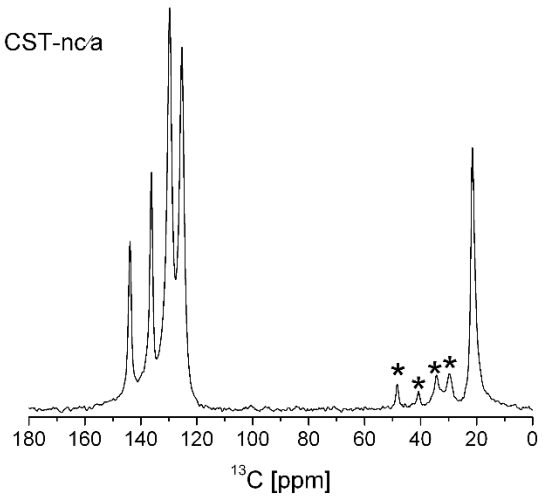

Figure S7. ^{13}C CP MAS NMR spectrum of CST-nc/a. Spinning sidebands are labeled with asterisks.

The spectra of the carbonized/activated materials are considerably different and exhibit much broader resonances (Figure S8), which is consistent with the disordered nature of these materials. The ^{13}C NMR spectra of the CT-1, CST-1 and CST-0 materials display essentially three regions at ca. 139, 129 and 20 ppm with varying levels of intensities. The resonance at 129 ppm is assigned to polycyclic aromatic carbons and/or to those adjacent to sulfonic acid groups; that at 20 ppm corresponds to the methyl group within the precursor molecule.[15,22] The spectrum of CT-1 shows a resonance at 150 ppm assigned to phenolic OH groups. The spectra of CST-1, CST-0-600 and CT-1 show much weaker resonances at 20 ppm in comparison to the resonance at 129 ppm than the spectrum of CST-0. These results suggest that pyrolysis was more extensive for the former materials, which is in agreement with the FT-IR data discussed above. Nevertheless, activation has important advantages compared to carbonization at 600 °C, such as the lower synthesis temperature and much better retention of the sulfur-containing groups.

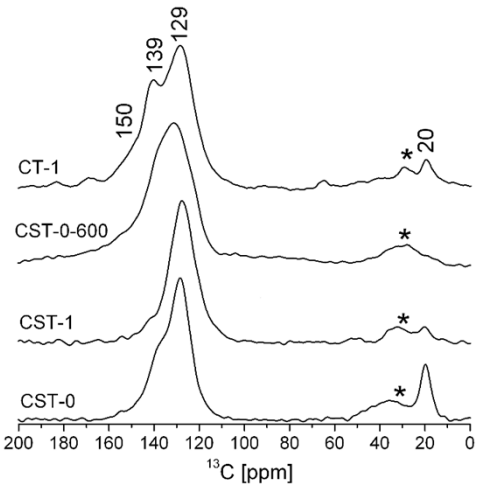

Figure S8. ^{1}H-^{13}C CP MAS spectra of prepared materials (sidebands are marked with an asterisk).

7. High resolution XPS of the prepared composite materials

Table S1. Relative percentage of S-containing functional groups obtained by fitting the S 2p XPS spectra.

Sample	SH	SO_3H	SH/SO_3H
CST-0	40.04	59.96	0.67
CST-0.1	51.06	48.94	1.04
CST-0.4	36.97	63.03	0.59
CST-1	18.03	81.97	0.22

Table S2. Relative percentage of functional groups obtained by fitting the C 1s XPS spectra.

Sample	C-C	C-O	C=O	COOH
CST-0	87.07	10.06	1.85	1.01
CST-0.1	87.24	9.48	2.24	1.04
CST-0.4	85.38	10.17	2.67	1.78
CST-1	73.74	15.17	6.22	4.86

8. ^{31}P MAS NMR deconvolution fittings of the selected CT and CST materials

Table S3. Deconvolution parameters obtained from the ^{31}P NMR spectra given in Figure 7.

Resonance (δ_{iso})	Percentage (%)
CT-1	
48.0 ± 0.20	4.0
57.0 ± 0.30	12.0
65.0 ± 0.02	24.0
73.1 ± 0.05	30.0
86.3 ± 0.06	28.0
100.1 ± 0.30	2.0
CST-0	
58.0 ± 0.30	8.0
64.0 ± 0.40	7.0
76.0 ± 0.30	31.0
80.0 ± 0.40	20.0
85.0 ± 0.20	28.0
97.0 ± 0.40	6.0
CST-0.1	
48.5 ± 1.00	8.0
61.0 ± 0.02	56.0
72.7 ± 0.08	8.0
81.0 ± 0.23	27.0
97.4 ± 0.50	1.0
CST-0.4	
46.0 ± 1.00	4.0
61.4 ± 0.10	37.0
73.2 ± 0.10	11.0
83.5 ± 0.10	44.0
98.0 ± 0.20	4.0
CST-1	
48.0 ± 0.40	1.0
61.2 ± 0.30	9.0
76.1 ± 0.30	26.0
88.3 ± 0.02	58.0
100.2 ± 0.10	6.0

9. Catalytic studies

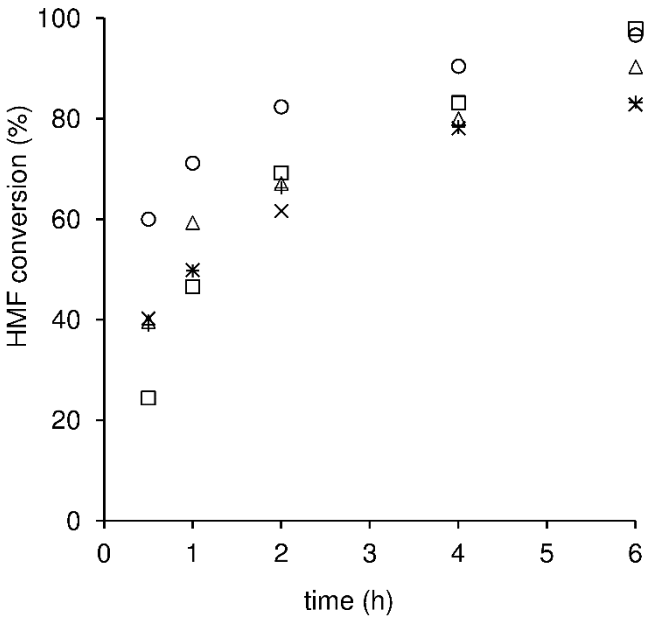

Figure S9. Kinetic profiles of the reaction of HMF, in the presence of CST-0.1 (□), CST-0.4 (Δ) or CST-1 (o), CT-1 (+) or Amberlyst-15 (×), using the same initial molar ratio of HMF/AS=50. Reaction conditions: $[HMF]_0$=0.33 M; 110 ºC.

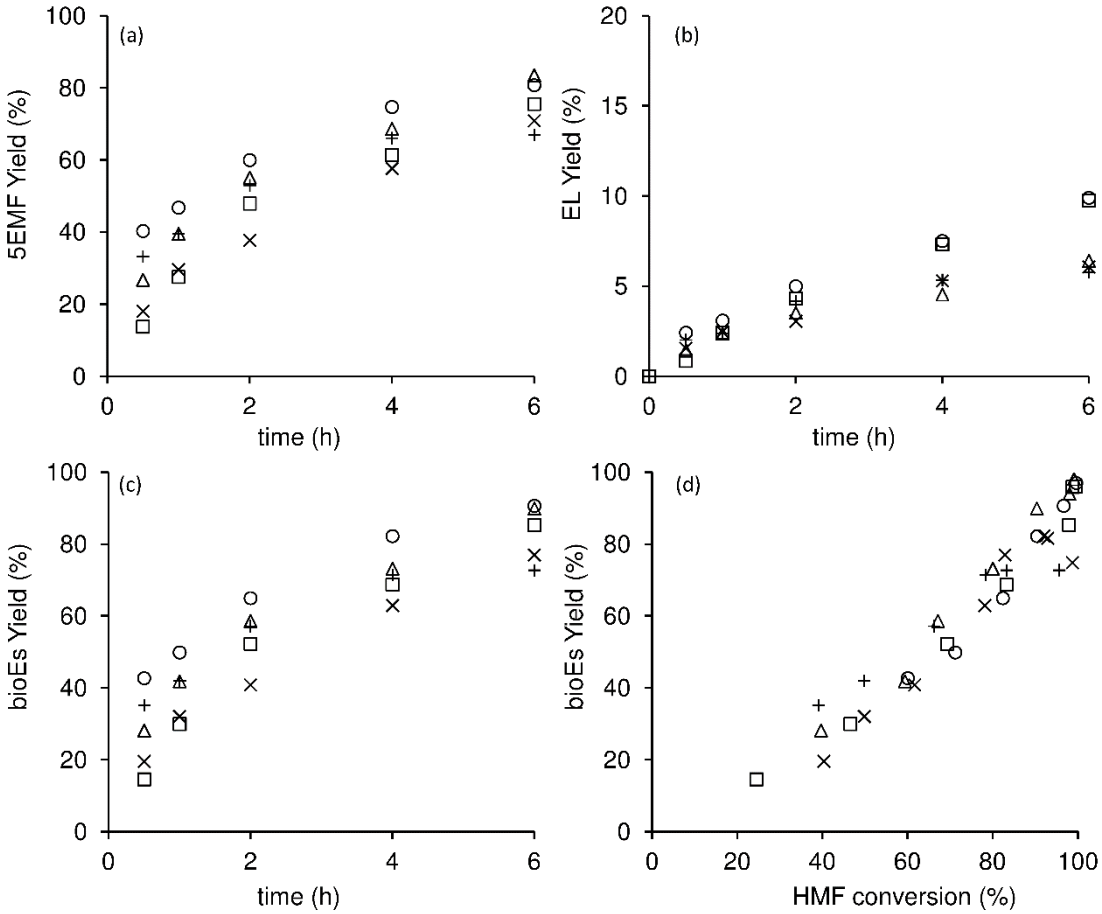

Figure S10. Dependence of the yields of (a) 5EMF, (b) EL (+, o, Δ, □) and (c) bioEs yield on reaction time, and (d) bioEs on HMF conversion, in the presence of CST-0.1 (□), CST-0.4 (Δ) or CST-1 (o), CT-1 (+) or Amberlyst-15 (×), using the same initial molar ratio of HMF/AS=50. Reaction conditions: $[HMF]_0$=0.33 M; 110 ºC.

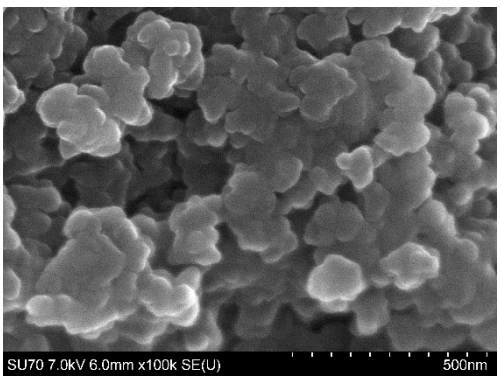

Figure S11. SEM image of powdered Amberlyst-15.

Table S4. Comparison of the catalytic results for CST-1 to those reported in the literature for various catalysts tested in the reaction of HMF with ethanol.

Catalyst [a]	Reaction conditions [b]				Conv.[c] (%)	bioEs yield (%)	Ref.
	T (ºC)	$[HMF]_0$ (M)	Cat. load ($g_{cat}.dm^{-3}$)	t (h)			
CST-1	140	0.33	10	1	100	96	-
CST-1	110	0.33	10	4	99	97	-
CST-1	110	1.29	20	4	96	95	-
S-RGO	140	0.33	10	2	99	95	1
S-RGO	110	0.33	10	4	98	96	1
S-GO	100	0.5	20	12	96	92	3
S-GO	100	0.5	10	12	85	83	3
S-CNT	140	0.33	10	24	99	86	1
S-CB	140	0.33	10	24	99	85	1
Amberlyst-15	110	0.33	1.5	24	92	82	-
Amberlyst-15	110	0.33	10	24	100	92	1
H-beta	110	0.33	10	4	67	56	-
Al-TUD-1(21)	110	0.3	10	4	98	96	4
Al-MCM-41(25)	140	0.7	n.m.	5	100	84	5
Al-MCM-41(50)	140	0.7	n.m.	5	100	78	5
Al-SBA-15	140	0.7	n.m.	5	75	-	5
ZrO_2/SBA-15	140	0.7	n.m.	5	100	99	5
SO_4^{2-}/ZrO_2/SBA-15	140	0.7	n.m.	5	100	97	5
SO_3H-SBA-15	140	0.12	16	24	~ 100	~ 85	6
HMS-SO_3H	100	0.20	200	10	95	85	7
H-ZSM-5 (11.5)	140	0.12	16	24	~ 100	~87	6
H-Mordenite(10)	140	0.12	16	24	~ 100	~ 85	6
Silica sulfuric acid	75	0.39	4.3	24	100	68	8
H-Y	70	0.2	6	24	10	9	9
$H_4SiW_{12}O_{40}$/MCM-41	90	1.7	42	4	92	82	10
$[MimB(SO_3H)]_3PW_{12}O_{40}$	70	0.2	37.5	24	98	91	9

[a] Value in parenthesis (when applied) is the Si/Al molar ratio. [b] Reaction conditions: T=reaction temperature (ºC), $[HMF]_0$=initial molar concentration of HMF, Cat. load=catalyst loading, t=time of reaction (h), n.m.=not mentioned. [c] HMF conversion.

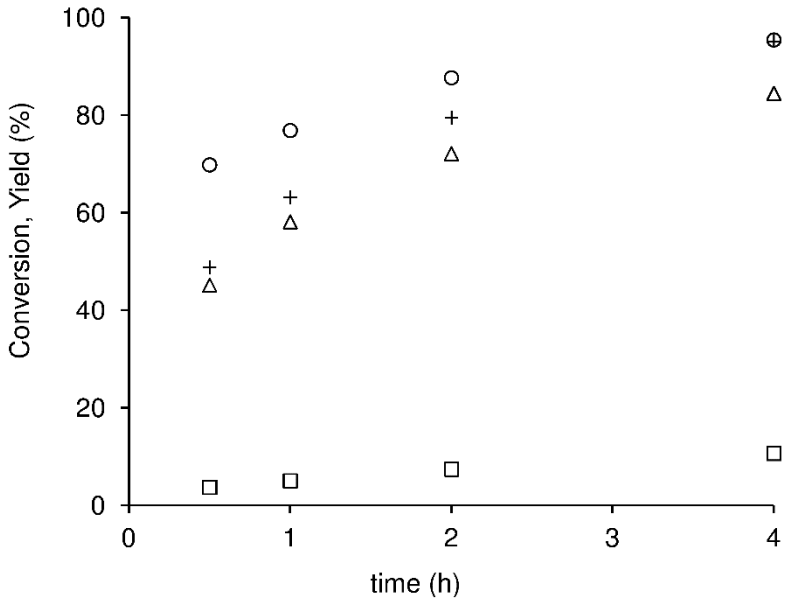

Figure S12. Kinetic profiles of HMF conversion (O), and dependence of the yields of 5EMF (Δ), EL (□) and bioEs (+) on reaction time, in the presence of CST-1. Reaction conditions: $[HMF]_0$=1.29 M; 10 mg catalyst, 0.5 mL ethanol, 110 ºC.

Table S5. Reaction of furfuryl alcohol with ethanol in the presence of the CST materials.[a]

Catalyst [a]	Reaction conditions		2EMF yield [c] (%)	EL yield [c] (%)
	T (ºC)	t (h)		
CST-0.1	110	16/24	8/4	77/86
CST-0.4	110	16/24	4/1	79/84
CST-1	110	16	-	82
CST-1	140	6	-	80

[c] FA conversion was always 100%. Reaction conditions: $[FA]_0$=0.33 M; catalyst loading=10 g_{cat} dm^{-3}.

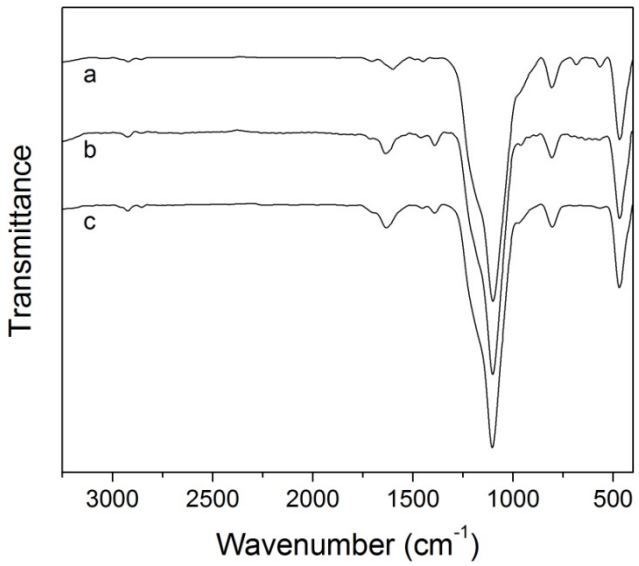

Figure S13. FT-IR spectra of a) CST-0, b) CST-0-ET and c) CST-0-WT.

References

1 M. M. Antunes, P. A. Russo, P. V. Wiper, J. M. Veiga, M. Pillinger, L. Mafra, D. V. Evtuguin, N. Pinna and A. A. Valente, *ChemSusChem,* 2014, **7**, 804-812.

2 S. Stankovich, D. A. Dikin, R. D. Piner, K. A. Kohlhaas, A. Kleinhammes, Y. Jia, Y. Wu, S. T. Nguyen and R. S. Ruoff, *Carbon,* 2007, **45**, 1558-1565.

3 H. Wang, T. Deng, Y. Wang, X. Cui, Y. Qi, X. Mu, X. Hou and Y. Zhu, *Green Chem.,* 2013*,* **15**, 2379-2383.

4 P. Neves, M. M. Antunes, P. A: Russo, J. P. Abrantes, S. Lima, A. Fernandes, M. Pillinger, S. M. Rocha, M. F. Ribeiro and A. A. Valente, *Green Chem.*, 2013, **15**, 3367-3376.

5 P. Lanzafame, D: M. Temi, S. Perathoner, G. Centi, A. Macario, A. Aloise and G. Giordano, *Catal. Today,* 2011, **175**, 435-441.

6 S. Saravanamurugan and A. Riisager, *Catal. Commun*., 2012, **17**, 71-75.

7 B. Liu and Z. Zhang, *RSC Adv*., 2013,. **3**, 12313-12319.

8 M. Balakrishnan, E. R. Sacia and A. T. Bell, *Green Chem.,* 2012, **14**, 1626-1634.

9 L. Bing, Z. Zhang and K. J. Deng, *Ind. Eng. Chem. Res*., 2012*,* **51**, 15331-15336.

10 P. Che, F. Lu, J. Zhang, Y. Huang, X. Nie, J. Gao and J. Xu, *Bioresour. Technol.,* 2012, **119**, 433-436.